CONFERENCE PRE-PRINT

ALPHA PARTICLE VELOCITY SPACE AND ORBIT SENSITIVITY OF GAMMA-RAY SPECTROSCOPY DIAGNOSTICS BASED ON THE $^{10}B(\alpha,p\gamma)^{13}C$ REACTION

M. NOCENTE[1,2*], A. CIURLINO[1], A. VALENTINI[3], H. JÄRLEBLAD[3], Y. KAZAKOV[4], V.G. KIPTILY[5], M. RUD[6], B. CORITON[7], G. CROCI[1], M. DALLA ROSA[1], S. FUGAZZA[1], G. GORINI[1], A. KOVALEV[7], G. MARCER[2], M. REBAI[2], M. TARDOCCHI[2] AND M. SALEWSKI[3]
[1] Dipartimento di Fisica "G. Occhialini", Università di Milano-Bicocca, Milan, Italy
[2] Institute for Plasma Science and Technology, National Research Council, Milan, Italy
[3]Department of Physics, Technical University of Denmark, Kgs. Lyngby, Denmark
[4]Laboratory for Plasma Physics, LPP-ERM/KMS Partner in the Trilateral Euregio Cluster (TEC), Brussels
[5]United Kingdom Atomic Energy Authority, Culham Campus, Abingdon, OX14 3DB, United Kingdom
[6]Swiss Plasma Center, École Polytechnique Fédérale de Lausanne, CH-1015 Lausanne, Switzerland
[7]ITER organization, St Paul Lez Durance Cedex, France.
*Corresponding author, email: massimo.nocente@mib.infn.it

Abstract

The study of burning plasmas, sustained by self-heating from fusion-born alpha particles, represents a critical milestone in nuclear fusion development. Upcoming devices such as ITER, SPARC, and BEST aim to explore this regime experimentally. A central challenge is the measurement of alpha particle phase space, which is essential for understanding burning plasma physics but remains experimentally demanding. Gamma-ray spectroscopy offers a powerful diagnostic by exploiting nuclear reactions between alpha particles and plasma impurities. Previous demonstrations at JET relied on beryllium-based reactions, but these are no longer applicable with ITER adoption of tungsten walls. As an alternative, boron reactions can be employed, despite their lower cross-sections. This work presents the first evaluation of velocity-space sensitivities for boron-based gamma-ray spectroscopy and compares them to beryllium-based diagnostics. The results demonstrate that boron-induced reactions can provide effective access to alpha particle velocity and orbit space, offering valuable guidance for the optimization of ITER's diagnostic design.

1. INTRODUCTION

A central mid-term objective in the development of nuclear fusion as an energy source is the study of *burning plasmas*—a regime in which plasma sustainment is primarily driven by self-heating from alpha particles produced in deuterium–tritium fusion reactions (Salewski & al., 2025). This is a key mission of ITER, the largest publicly funded tokamak under construction in France, as well as complementary private and public–private efforts such as SPARC in the USA and BEST in China.

A full understanding of burning plasma physics requires accurate measurement of the alpha particle phase space, a task long recognized as essential but experimentally challenging. It demands the integration of multiple diagnostic techniques. Among the few proven approaches, gamma-ray spectroscopy can access the alpha particle phase space by detecting characteristic line emissions from spontaneous nuclear reactions between alpha particles and plasma impurities (Kiptily & al., 2002) (Nocente & al., 2020).

With ITER and other forthcoming devices adopting tungsten as the first-wall material, beryllium—previously used in gamma-ray spectroscopy diagnostics—will no longer be available. Instead, boron impurities, either introduced deliberately for wall conditioning or present as residuals, provide an alternative. This work presents, for the first time, the velocity-space and orbit sensitivity of alpha particle measurements based on gamma-ray emission from alpha–boron reactions.

Gamma-ray spectroscopy has been established primarily at the Joint European Torus (JET) to probe energetic ion populations, relying on reactions with either ^{12}C or ^{9}Be impurities depending on the first-wall composition over its operational lifetime. In recent deuterium–tritium campaigns (DTE2 and DTE3) with a beryllium wall, alpha particle measurements were successfully demonstrated using both high-purity germanium detectors (Kiptily & al., 2024) and $LaBr_3(Ce)$ scintillators (Nocente & al., 2022). These measurements exploited the 4439 keV line from the $^{9}Be(\alpha,n\gamma)^{12}C$ reaction with naturally occurring ^{9}Be impurities at ~1% concentration in JET plasmas.

On the theoretical side, methods have been developed to quantify velocity-space sensitivity in terms of *weight functions,* which quantify the sensitivity of the diagnostic in phase space or velocity space, i.e. they show the detectable signal per ion for any location in velocity- or phase space.
Following ITER's re-baselining, no planned burning plasma device will employ beryllium walls, necessitating alternative nuclear reactions for alpha particle measurements via gamma-ray spectroscopy. A promising candidate is the $^{10}B(\alpha,p\gamma)^{13}C$ reaction, expected when boron impurities are present, e.g. from wall conditioning. Although its cross section is smaller than that of $^{9}Be(\alpha,n\gamma)^{12}C$, this reaction produces three distinct emission lines (3089, 3684, and 3854 keV), thereby offering in principle enhanced velocity-space diagnostic capability.
Building on a recent detailed evaluation of the relevant cross sections (Kiptily V. , 2025), we present here the first calculations of velocity-space sensitivities for boron-based gamma-ray spectroscopy.
This conference manuscript is organized as it follows. Section 2 summarizes the nuclear and cross section data of the $^{10}B(\alpha,p\gamma)^{13}C$ reaction. Section 3 provides a comparative calculation of the shapes of the gamma-ray emission lines from the $^{10}B(\alpha,p\gamma)^{13}C$ and $^{9}Be(\alpha,n\gamma)^{12}C$ reactions when the alpha particle distribution function is given from a simple analytical model. Weight functions are introduced in section 4 and 5, where first results for the $^{10}B(\alpha,p\gamma)^{13}C$ reaction are provided.

2. NUCLEAR AND CROSS SECTION DATA FOR THE $^{10}B(\alpha,p\gamma)^{13}C$ REACTION

In the $^{10}B(\alpha,p\gamma)^{13}C$ reaction alpha particles, that interact with ^{10}B impurities, lead to the production of the ^{13}C nucleus in its ground state or in one of its excited states. When the latter occurs, gamma-rays at discrete energies (lines) are produced.
Figure 1 shows the first three excited states of the ^{13}C nucleus. The first level (L1) is found at an energy E=3089 keV and, when populated, has a 100% probability of emitting a gamma-ray at the energy E_γ=3089 keV. There is then a second excited state (L2) at the energy E=3685 keV and that also decays exclusively by gamma-ray emission, leading to E_γ=3685 keV. The decay mode of the third excited (L3) state is more complicated. There is a 63% probability for L3 to decay by gamma-ray to L2, leading to a low energy gamma-ray of 169 keV, which is experimentally hard to distinguish from the background. On the other hand, when this happens, within nanoseconds L2 decays towards the ground state (GS), contributing to the E_γ=3685 keV emission. In other words, experimentally the E_γ=3685 keV emission is a combined contribution of a direct decay from L2 (100% probability) and a cascade decay from L3 (63% probability). Finally, L3 has a 37% probability to decay by gamma-ray emission to the ground state, leading to E_γ=3854 keV.

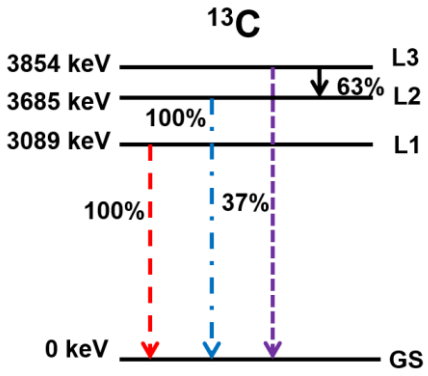

Figure 1 Level scheme of the ^{13}C nucleus born in the $^{10}B(\alpha,p\gamma)^{13}C$ reaction.

The total cross section to populate each excited state depends on the alpha particle energy and is different for each nuclear level, see Figure 2, which combines data from (Liu & al., 2020) for E_α< 1.8 MeV and data from (Kiptily V. , 2025) for higher energies up to $E_\alpha\approx$4 MeV. The cross section to populate the first excited state of ^{12}C in the $^{9}Be(\alpha,n\gamma)^{12}C$ reaction, and primarily responsible for the emission of E_γ=4.44 MeV used for alpha

particle studies, is shown to the right for comparison. We find that the $^{10}B(\alpha,p\gamma)^{13}C$ has a generally lower cross section than $^{9}Be(\alpha,n\gamma)^{12}C$ and the most dominant emissions expected to be measured are those at E_γ=3854 keV and E_γ=3685 keV.

For the evaluation of the differential cross section in the c.m. frame $d\sigma/d\Omega_{c.m.}$, which has an impact of the shape of the gamma-ray emission lines (Nocente M. , PhD Thesis, 2012) and, thus, on the corresponding weight functions, we have used the data on the A_k coefficients available in (Kiptily V. , 2025) and expressed $d\sigma/d\Omega_{c.m}$ as:

$$\frac{d\sigma}{d\Omega_{c.m.}} = \frac{\sigma_{TOT}}{4\pi} + \sum_k A_k P_k(cos\theta_{c.m.}) \quad (1)$$

where σ_{TOT} is the total reaction cross section, P_k are Legendre polynomials of order k and $\cos\theta_{c.m.}$ is the cosine of the proton angle in the c.m. frame.

Figure 3 shows an example of the differential cross section to populate L3 for E_α=1,2 and 3 MeV using the equation above. The cross section is isotropic in the c.m. frame in the energy range where data from (Liu & al., 2020) are available, while a non-trivial anisotropy, which changes depending on E_α, is seen for energies above ≈ 2 MeV, where data from (Kiptily V. , 2025) are available instead.

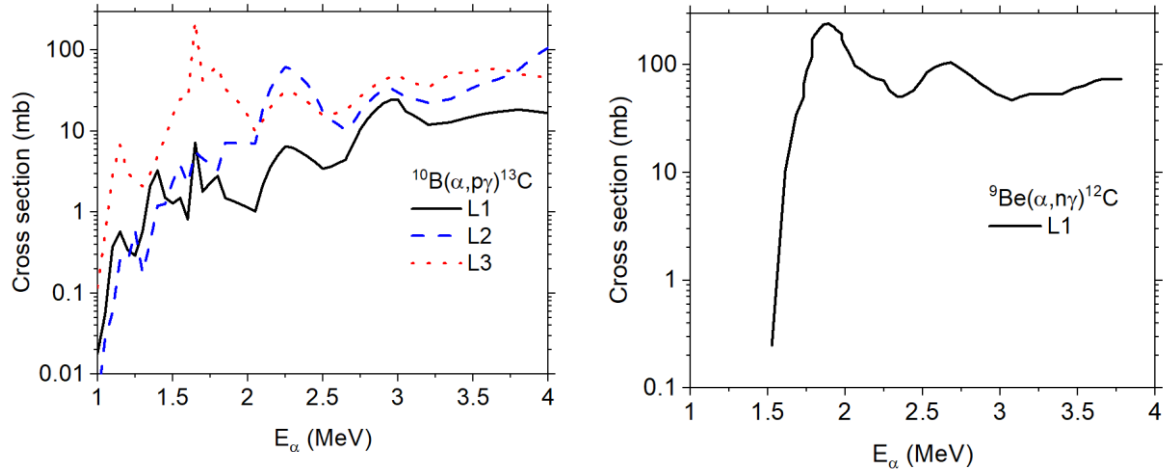

Figure 2 (left) Total cross section to populate the three ^{13}C excited states born from the $^{10}B(\alpha,p\gamma)^{13}C$ cross section. (right) Total cross section to populate the first excited state born from the $^{9}Be(\alpha,n\gamma)^{12}C$ cross section.

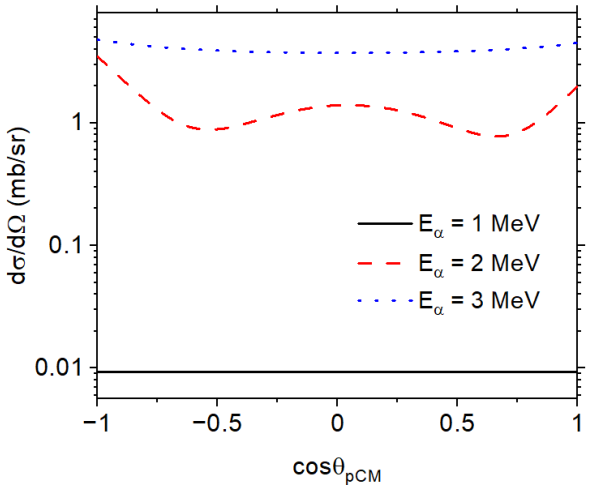

Figure 3: Differential cross section for L3 of the ^{13}C nucleus born from the $^{10}B(\alpha,p\gamma)^{13}C$ reaction and as a function of the alpha particle energy E_α.

3. GAMMA-RAY PEAK SHAPES

Using the differential cross section data above, we can now make a first calculation of the expected shape of the 3 gamma-ray lines born from the $^{10}B(\alpha,p\gamma)^{13}C$ reaction and compare the results with the shape of the 4.44 MeV gamma-ray line born from $^{9}Be(\alpha,n\gamma)^{12}C$. In all cases, we assume that the alpha particle distribution function $f_\alpha(v)$ is isotropic and given by ***(Trubnikov, 1965)***

$$f_\alpha(v) = \frac{\tau_s}{v^3+v_C^3}\int_0^{+\infty} S(v)dv \quad (2)$$

where τ_s is the Spitzer slowing down time, v_C the critical velocity and S(v) the velocity spectrum of the alpha particles per second and cubic meter that are generated by the d+t fusion reaction. The latter is computed with GENESIS ***(Nocente M. , PhD Thesis, 2012)***. For simplicity, the plasma is assumed to be uniform with equal ion and electron temperature set to 20 keV and an electron density of 10^{20} m^{-3}. Furthermore, the tritium and deuterium isotope concentrations are the same, while the concentration of the reaction impurity (^{9}Be or ^{10}B) is assumed to be 1% with respect to the electron density.

Figure 4 shows the result of the calculations. To aid the comparison of the peak shapes, the x axis is normalized to the nominal gamma-ray energy $E_{\gamma 0}$ for each emission and the shapes are normalized to have the same maximum. For simplicity, in this first calculation we have neglected the contribution of L3 to the E_γ=3685 keV line. Although the same alpha particle distribution function is used in the calculations, the peak shapes are different, suggesting that, depending on the line, different alpha particle energies are manifested in the emissions. We also note that the broadening of the peak shapes with respect to their nominal energy is at the level of ≈ 1% (full width at half maximum) for all the lines. This suggests that such broadening is unlikely to be measurable with inorganic scintillators, such as $LaBr_3$(Ce) (Nocente & al., 2010), as these detectors typically feature an energy resolution of a few percents at MeV range energies. On the other hand, measurements of such peak shape broadening are within the capability of high purity germanium detectors (Nocente & al., 2020), as they have an intrinsic detector broadening of < 0.1%.

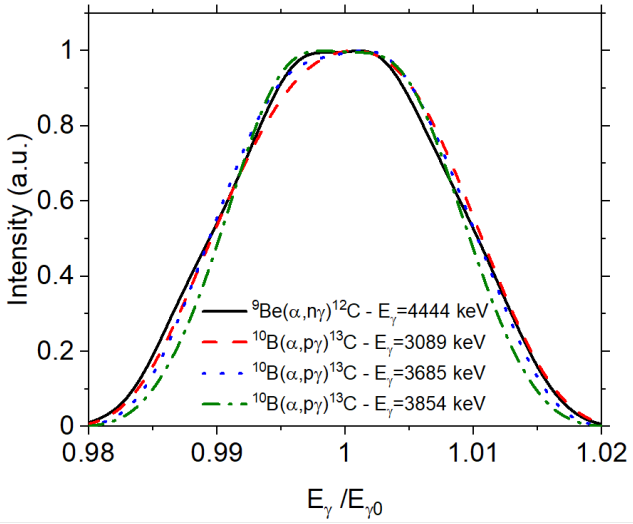

Figure 4: Peak shapes of the 3 gamma-ray lines at $E_{\gamma 0}$=3089 keV, $E_{\gamma 0}$=3685 keV and $E_{\gamma 0}$=3854 keV from the $^{10}B(\alpha,p\gamma)^{13}C$ reaction for alpha particles born from the d+t fusion reaction. The shape of the $E_{\gamma 0}$=4444 keV line from the $^{9}Be(\alpha,n\gamma)^{12}C$ reaction is also shown for comparison. Peak shapes are normalized to have the same height. The x axis is also normalized by the nominal gamma-ray energy.

4. VELOCITY SPACE WEIGHT FUNCTIONS

Weight functions, here denoted as *w*, connect two-dimensional fast-ion distribution functions, *f*, to measurements, *s,* according to

$$s(E_{\gamma 1}, E_{\gamma 2}, \phi) = \int_{Volume} \quad \int_0^{+\infty} \quad \int_{-\infty}^{+\infty} w(E_{\gamma 1}, E_{\gamma 2}, \phi, v_{\parallel,} v_{\perp}, x) f(v_{\parallel}, v_{\perp}, x) dv_{\parallel} dv_{\perp} dx$$

For Gamma-Ray Spectroscopy (GRS) measurements (Salewski & al., 2015), $s(E_{\gamma 1},E_{\gamma 2},\varphi)$ represents the detection rate of γ-rays [photons/s] within the energy interval $E_{\gamma 1}<E<E_{\gamma 2}$, observed at a viewing angle φ between the GRS line-of-sight and the magnetic field. Here, $(v_{\parallel},v_{\perp})$ are the velocity components parallel and perpendicular to the magnetic field, respectively. We employ the two-dimensional $(v_{\parallel},v_{\perp})$ coordinate system instead of the more commonly used (energy, pitch)-coordinates since results are better understood in $(v_{\parallel},v_{\perp})$. The fast-ion velocity distribution function f reduces to a 2D form due to the rotational symmetry of the full 3D distribution, as distribution functions do not depend on the gyroangle owing to the rotation symmetry around the field lines.
In cylindrical coordinates, $v_{\parallel}$ can take both positive and negative values, whereas $v_{\perp}$ is always positive. The units of f in equation (4) are $[s^2m^{-5}]$. Consequently, the units of GRS weight functions are [photons/(α-particle×s]. We here neglect the spatial dependence of *w*, as gamma-ray emission primarily comes from the plasma core.
Weight functions for any fast-ion diagnostic, including GRS, can be determined numerically using a forward model capable of predicting the measurement for an arbitrary fast-ion distribution. In this method, we calculate γ-ray energy spectra emitted from a test population of N_f fast alpha particles, with their velocities $(v\parallel,v\perp)$ varied systematically to scan the relevant region of velocity space. This was done here with the GENESIS code (Nocente M. , PhD Thesis, 2012), as described in (Salewski & al., 2015).
Figure 5 to Figure 7 show the velocity space weight functions associated to the three gamma-ray lines E_{γ}=3089 keV, 3685 keV and 3854 keV from the $^{10}B(\alpha,p\gamma)^{13}C$ reaction and when the observation angle is ϕ=90°. Weight functions are shown for spectral channels that are Doppler shifted by ΔE_{γ}=-15,0, +15, +30, +45 and +60 keV with respect to the nominal gamma-ray energy $E_{\gamma 0}$. For simplicity, we have neglected the contribution of the cascade transition from L3 to the E_{γ}=3685 keV line. As already suggested by the spectral shape of Figure 4, there are differences among the weight functions associated to the different lines. For the L1 emission, there is primarily a combined sensitivity to $v_{\alpha}\approx 1.2\text{x}10^7$ m/s and v_{α} in the range between $1.4\text{x}10^7$ m/s and $1.6\text{x}10^7$ m/s for energy channels near the nominal energy and below. The sensitivity becomes more and more restricted to the $1.3\text{x}10^7$ m/s and $1.6\text{x}10^7$ m/s velocity range as one moves towards the high energy region of the spectral shape. For the L2 emission, the sensitivity is dominated by v_{α} in the range between $1.4\text{x}10^7$ m/s and $1.6\text{x}10^7$ m/s in practically all the energy channels, with a minor contribution by alpha particles having $v_{\alpha}\approx 1.0\text{x}10^7$ m/s close to the nominal energy of the emission. As for L3, the sensitivity qualitatively changes in a way similar to L1, but with different values of $v_{\alpha,}$ i.e. $\approx 0.9\text{x}10^7$ m/s close to the peak nominal energy and in the range $1.3\text{x}10^7$ m/s to $1.6\text{x}10^7$ m/s, both around the nominal energy and for the higher energy channels. As found for the $^9Be(\alpha,n\gamma)^{12}C$ reaction (see (Salewski & al., 2015), weight functions for ϕ=90° are symmetric when the sign of the parallel velocity is flipped. For a given v_{α}, the sensitivity to changes of the pitch angle are similar for all the emissions. The signal around the peak nominal energy is dominated by particles with a higher component of the parallel velocity, both parallel and anti-parallel to the magnetic field. For higher energy channels, the sensitivity is dominated by particles that have predominantly a velocity perpendicular to the magnetic field.
Weight functions for an observation angle ϕ=30° are shown in Figure 8 and for the L3 emission only. As found for the $^9Be(\alpha,n\gamma)^{12}C$ reaction, weight functions are in this case asymmetric and the sensitivity shifts from alpha particles with $v_{\perp} \gg v_{\parallel}$ to particles with $v_{\parallel} \gg v_{\perp}$ as one moves from channels around the nominal peak energy to the high energy tail of the peak. The energy sensitivity of the weight functions does not substantially depend on the observation angle, instead.
Compared to the weight functions of the $^9Be(\alpha,n\gamma)^{12}C$ reaction, which depended on a larger range of alpha particle velocities, weight functions of the $^{10}B(\alpha,p\gamma)^{13}C$ seem to have a higher selectivity in the velocity space, which is also enhanced by the possibility to observe, in principle, three lines, rather than one. On the other hand, the cross section of boron based reaction is, in general, lower by about a factor 2 than that of beryllium based processes, which experimentally implies that correspondingly ≈2 times longer integration times may be required to achieve data with the same statistical quality than those that could be obtained from $^9Be(\alpha,n\gamma)^{12}C$.

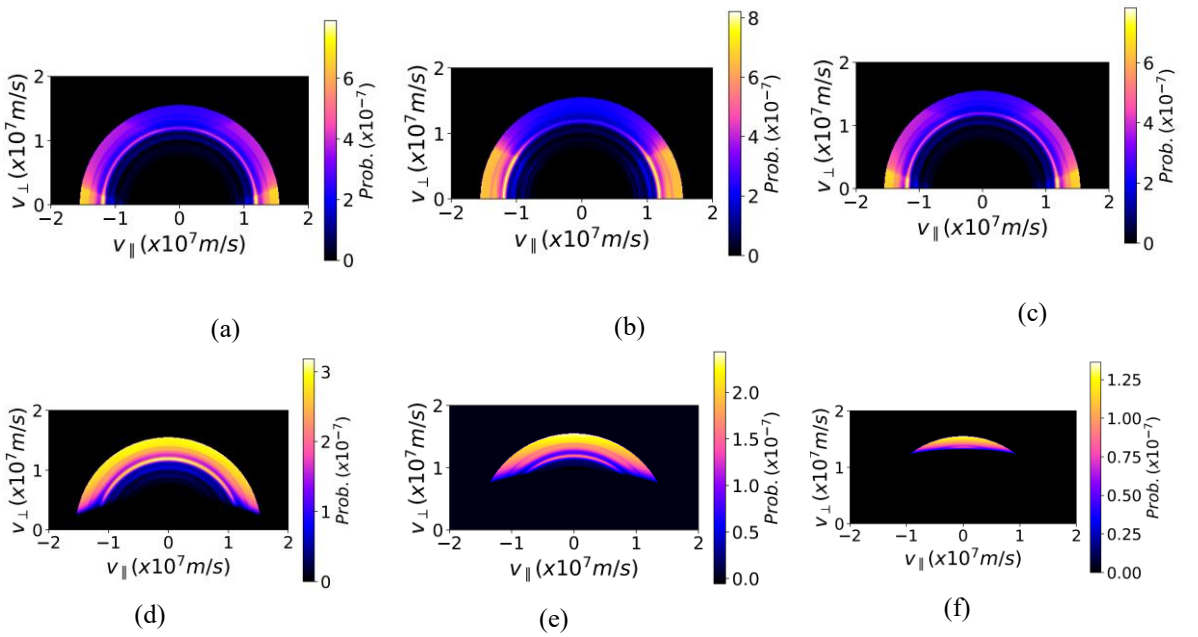

Figure 5: Numerical GRS weight functions *w* (photons/(*α*-particle × s)) for ϕ = 90° and various Doppler-shifted energies E_γ of the *γ*-photons from the L1 emission of ^{13}C born from the $^{10}B(\alpha,p\gamma)^{13}C$ reaction . The *γ*-ray energy bin width is ΔE_γ=1 keV. Each panel corresponds to a different energy channel E_γ with respect to the nominal gamma-ray energy $E_{\gamma 0}$=3089 keV and identified by their energy shift ΔE_γ=-15 keV (a), 0 keV (b), 15 keV (c), 30 keV (d), 45 keV (e), 60 keV (f) .

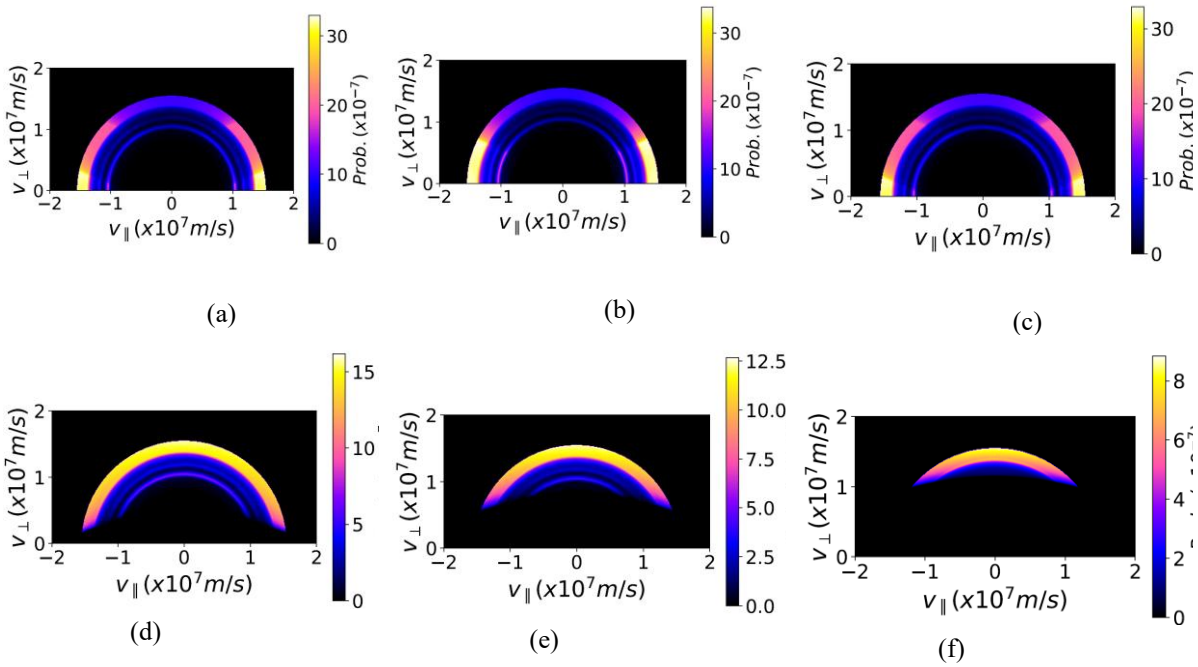

Figure 6: Numerical GRS weight functions *w* (photons/(*α*-particle × s)) for ϕ = 90° and various Doppler-shifted energies E_γ of the *γ*-photons from the L2 emission of ^{13}C born from the $^{10}B(\alpha,p\gamma)^{13}C$ reaction . The *γ*-ray energy bin width is ΔE_γ=1 keV. Each panel corresponds to a different energy channel E_γ with respect to the nominal gamma-ray energy $E_{\gamma 0}$=3685 keV and identified by their energy shift ΔE_γ=-15 keV (a), 0 keV (b), 15 keV (c), 30 keV (d), 45 keV (e), 60 keV (f).

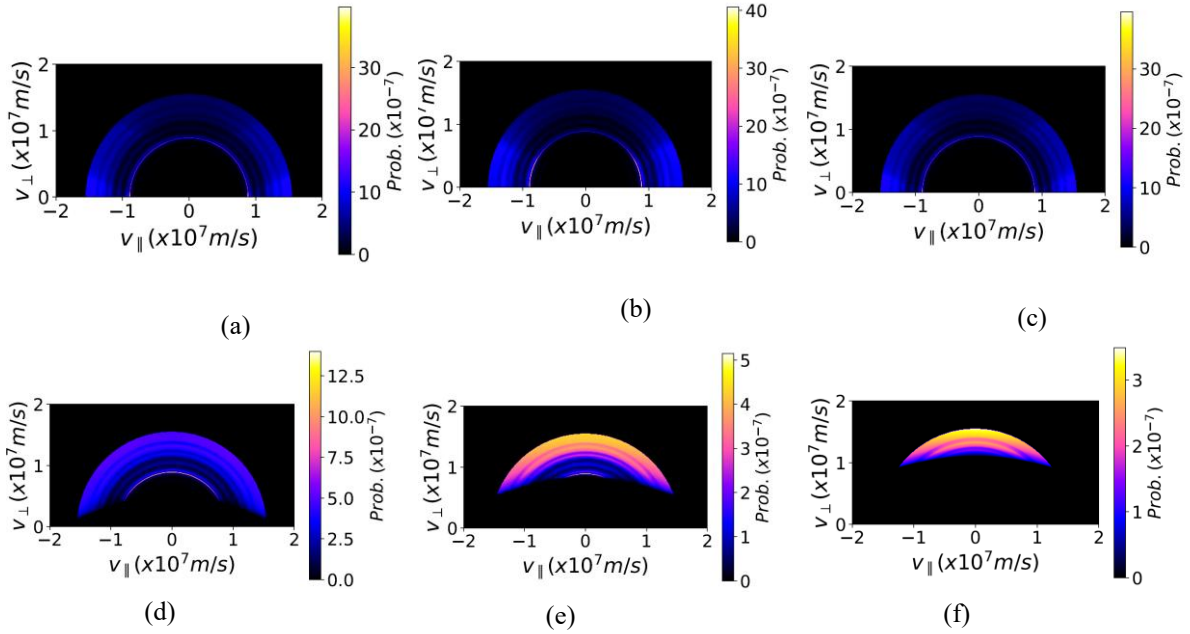

Figure 7: Numerical GRS weight functions *w* (photons/(*α*-particle × s)) for ϕ = 90° and various Doppler-shifted energies E_γ of the *γ*-photons from the L3 emission of ^{13}C born from the $^{10}B(\alpha,p\gamma)^{13}C$ reaction . The *γ*-ray energy bin width is ΔE_γ=1 keV. Each panel corresponds to a different energy channel E_γ with respect to the nominal gamma-ray energy $E_{\gamma 0}$=3854 keV and identified by their energy shift ΔE_γ=-15 keV (a), 0 keV (b), 15 keV (c), 30 keV (d), 45 keV (e), 60 keV (f).

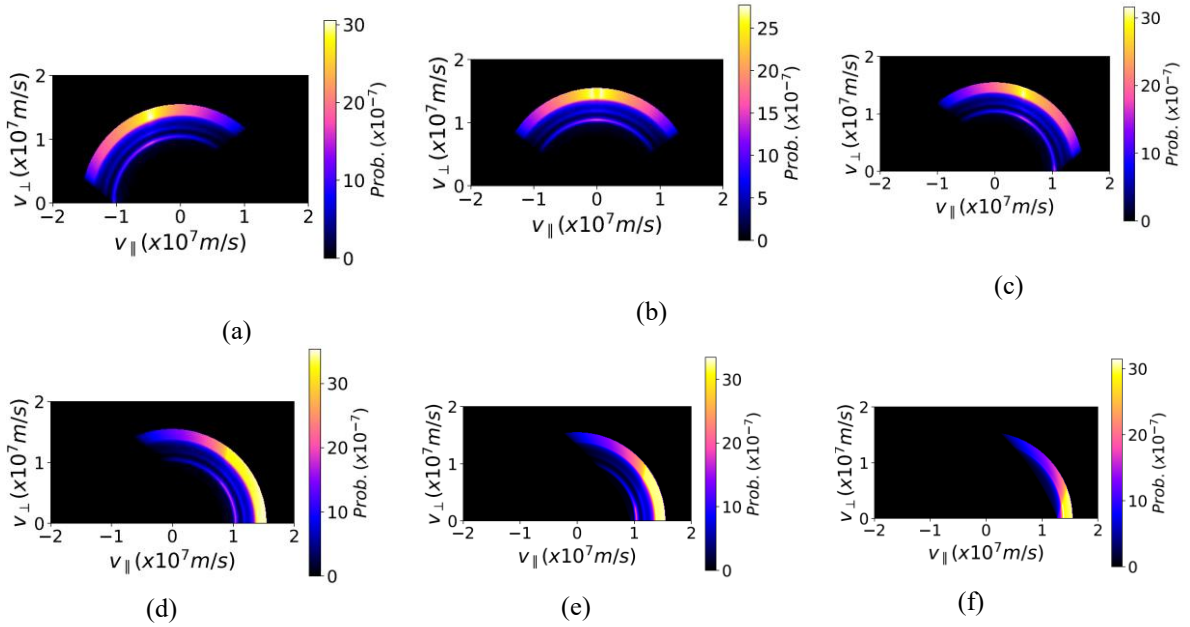

Figure 8: Numerical GRS weight functions *w* (photons/(*α*-particle × s)) for ϕ = 30° and various Doppler-shifted energies E_γ of the *γ*-photons from the L3 emission of ^{13}C born from the $^{10}B(\alpha,p\gamma)^{13}C$ reaction . The *γ*-ray energy bin width is ΔE_γ=1 keV. Each panel corresponds to a different energy channel E_γ with respect to the nominal gamma-ray energy $E_{\gamma 0}$=3685 keV and identified by their energy shift ΔE_γ=-15 keV (a), 0 keV (b), 15 keV (c), 30 keV (d), 45 keV (e), 60 keV (f).

5. ORBIT SPACE WEIGHT FUNCTIONS

Besides velocity space weight functions, orbit weight functions have been recently developed also for GRS (Valentini & al., 2025) and the $^{9}Be(\alpha,n\gamma)^{12}C$ reaction. These enable the representation of the diagnostic sensitivity in phase spaces, that combine both position and velocity and allow one to capture geometric effects (such as detector line-of-sight) as well as spatial gradients in important plasma parameters like density and temperature of the reacting species. More importantly, orbit weight functions (Stanger & Heidbrink, 2017) (Järleblad & al., 2022) connect the diagnostic observations directly to the fast-ion guiding-centre orbits, that are key to understand the interplay between plasma instabilities and fast-ion confinement (Salewski & al., 2025).
At the time of writing this conference manuscript, orbit weight functions for the three emissions of the $^{10}B(\alpha,p\gamma)^{13}C$ are under evaluation. Results will be presented in a comprehensive publication on the sensitivity of boron-based GRS to the velocity and orbit space of the alpha particles following this conference.

6. CONCLUSIONS

The first evaluation of velocity-space sensitivities for boron-based GRS, and a comparison with beryllium-based GRS, has been made in this work. The results demonstrate that boron-induced reactions can provide effective access to alpha particle velocity and a generally better alpha particle selectivity compared to ^{9}Be based processes. The sensitivity to the alpha particle pitch depends on the observation angle and is similar for the two cases. Concerning the magnitude of the emission, boron-based GRS is expected to have a factor 2 lower intensity than ^{9}Be-based GRS, due to the lower cross sections.
Calculations of the orbit space sensitivity of GRS have recently been made for the $^{9}Be(\alpha,n\gamma)^{12}C$ and are now being extended also to boron-based reactions. Results will be presented in a comprehensive publication on the sensitivity of boron-based GRS to the velocity and orbit space of the alpha particles following this conference.

ACKNOWLEDGEMENTS

The views and opinions expressed herein do not necessarily reflect those of the ITER Organization.

REFERENCES

Järleblad, H., & al. (2022). *Nucl. Fusion*, 62 112005.
Kiptily, V. (2025). *Fusion Engineering and Design*, 114959.
Kiptily, V., & al. (2002). *Nucl. Fus.*, 42 999.
Kiptily, V., & al. (2024). *Nucl. Fusion*, 64 086059.
Liu, & al. (2020). *Physical Review C*, 025808.
Nocente, M. (2012). *PhD Thesis.*
Nocente, M., & al. (2010). *Rev. Sci. Instrum. 81*, 10D321.
Nocente, M., & al. (2020). *Plasma Phys. Control. Fusion*, 62 014015.
Nocente, M., & al. (2022). *Rev. Sci. Instrum.* , 93 093520.
Salewski, M., & al. (2015). *Nucl. Fusion*, 093029.
Salewski, M., & al. (2025). *Nucl. Fusion*, 043002.
Stanger, L., & Heidbrink, W. (2017). *Phys. Plasmas 24*, 092505.
Trubnikov, B. A. (1965). *Rev. Plasma Phys. 1*, 105.
Valentini, A., & al. (2025). *Nucl. Fusion*, 10.1088/1741-4326/ae013d.